AFRL-SR-AR-TR-09-0154

REPORT DOCUMENTATION PAGE

PLEASE DO NOT RETURN YOUR FORM TO THE ABOVE ORGANIZATION.

1. REPORT DATE *(DD-MM-YYYY)*	2. REPORT TYPE	3. DATES COVERED *(From - To)*
28-02-2009	Final	03/01/2006-02/28/2009

4. TITLE AND SUBTITLE
Towards High-Reynolds-Number Quiet Flow in Hypersonic Wind Tunnels

5a. CONTRACT NUMBER
FA9550-06-1-0182

5b. GRANT NUMBER

5c. PROGRAM ELEMENT NUMBER
61102F

6. AUTHOR(S)
Steven P. Schneider, Professor

5d. PROJECT NUMBER
2307A

5e. TASK NUMBER

5f. WORK UNIT NUMBER

7. PERFORMING ORGANIZATION NAME(S) AND ADDRESS(ES)
Purdue University
Aerospace Sciences Lab
1375 Aviation Drive West Lafayette, IN 47907-2015

8. PERFORMING ORGANIZATION REPORT NUMBER

9. SPONSORING/MONITORING AGENCY NAME(S) AND ADDRESS(ES)
AFOSR
875 N Randolph St
Arlington VA 22203
Dr John Schmisseur/NA

10. SPONSOR/MONITOR'S ACRONYM(S)

11. SPONSOR/MONITOR'S REPORT NUMBER(S)

12. DISTRIBUTION/AVAILABILITY STATEMENT
Distribution A

13. SUPPLEMENTARY NOTES

14. ABSTRACT
This grant was initially focused on developing high-Reynolds-number quiet °ow in thc Boeing/AFOSR Mach-6 Quiet Tunnel at Purdue. Reliable quiet °ow was achievcd at freestream unit Reynolds numbers of more than 3 million pcr foot, beginning in Sept. 2006. Thc facility became the only operational hypersonic quiet tunnel, anywhere in the world. Tunnel noise was then shown to have a substantial effect on: a) roughness-induced transition for the X-51A forebody and a slender cone, and b) transition induced by stationary cross flow waves. Quiet-tunnel mcasurements were also made to aid estimates of transition for the DARPA FALCON HTV-2 program [1]. Second-mode instability waves were measured on a slender cone using hot wires, fast pressure sensors, and ALTP heat-transfer gauges.

15. SUBJECT TERMS

16. SECURITY CLASSIFICATION OF:			17. LIMITATION OF ABSTRACT	18. NUMBER OF PAGES	19a. NAME OF RESPONSIBLE PERSON
a. REPORT	b. ABSTRACT	c. THIS PAGE		31	Steven P. Schneider
					19b. TELEPHONE NUMBER *(Includa area code)* 765-494-3343

Final Report for AFOSR Grant FA9550-06-1-0182

1 Mar. 2006 to 28 Feb. 2009

Towards High-Reynolds-Number Quiet Flow in Hypersonic Wind Tunnels

Steven P. Schneider, Professor
School of Aeronautics and Astronautics
Purdue University
Aerospace Sciences Lab
1375 Aviation Drive West Lafayette, IN 47907-2015

April 13, 2009

1 Summary

This grant was initially focused on developing high-Reynolds-number quiet flow in the Boeing/AFOSR Mach-6 Quiet Tunnel at Purdue. Reliable quiet flow was achieved at freestream unit Reynolds numbers of more than 3 million per foot, beginning in Sept. 2006. The facility became the only operational hypersonic quiet tunnel, anywhere in the world.

Tunnel noise was then shown to have a substantial effect on: a) roughness-induced transition for the X-51A forebody and a slender cone, and b) transition induced by stationary crossflow waves. Quiet-tunnel measurements were also made to aid estimates of transition for the DARPA FALCON HTV-2 program [1]. Second-mode instability waves were measured on a slender cone using hot wires, fast pressure sensors, and ALTP heat-transfer gauges. Preliminary measurements on the cone using fast pressure sensors show that reducing the tunnel noise from conventional to quiet levels reduced the amplitude of the second-mode waves near 250kHz by a factor of about 450; this factor is roughly 5-10 times larger than the ratio of the broad-band RMS pitot-pressure fluctuations. The laser differential interferometer was enhanced and moved from the old Mach-4 tunnel to the new Mach-6 tunnel. The glow discharge perturber has also been reconfigured for use in the Mach-6 tunnel [2]. In addition, a number of hypersonic-transition review papers were written, to help educate the next generation.

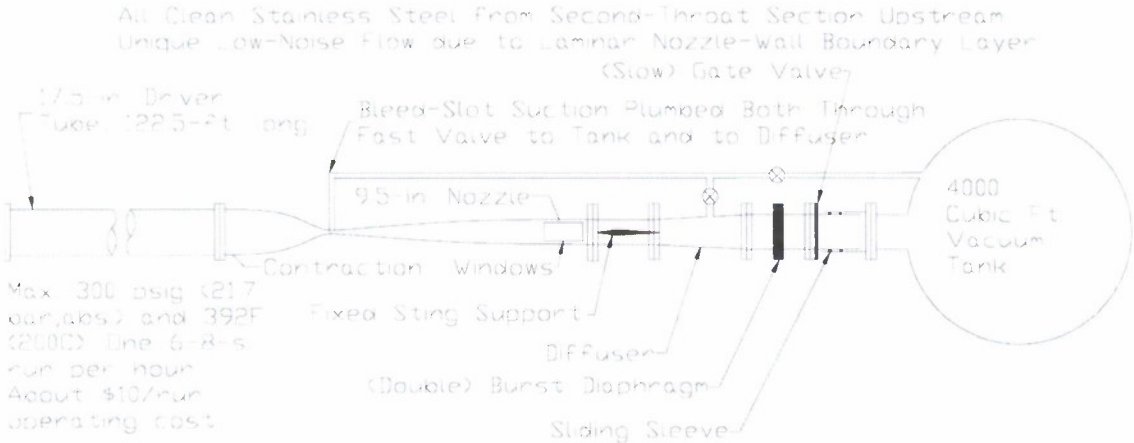

Figure 1: Schematic of Boeing/AFOSR Mach-6 Quiet Tunnel

2 Introduction

The work done under this grant is documented in a series of AIAA Papers [3, 4, 5, 6, 7, 8, 9, 10, 11, 2], and other conference papers [12, 13]. A series of review papers was also written, to educate a new generation of engineers not familiar with the vast Cold War literature [14, 15, 16, 17]. Several of these conference papers were revised into journal papers [18, 19, 20, 21, 22, 23, 24, 25, 26]. A number of students also completed their theses [27, 28, 29]. Since considerable detail is readily available in these publications, the present final report was written as an overall summary.

3 The Boeing/AFOSR Mach-6 Quiet Tunnel

Quiet facilities require low levels of noise in the inviscid flow entering the nozzle through the throat, and laminar boundary layers on the nozzle walls. To reach these low noise levels, conventional blow-down facilities must be extensively modified. Requirements include a 1 micron particle filter, a highly polished nozzle with bleed slots for the contraction-wall boundary layer, and a large settling chamber with screens and sintered-mesh plates for noise reduction [30]. To reach these low noise levels in an affordable way, the Purdue facility has been designed as a Ludwieg tube [31]. A Ludwieg tube is a long pipe with a converging-diverging nozzle on the end, from which flow exits into the nozzle, test section, and second throat, as shown in Fig. 1. A diaphragm is placed downstream of the test section. When

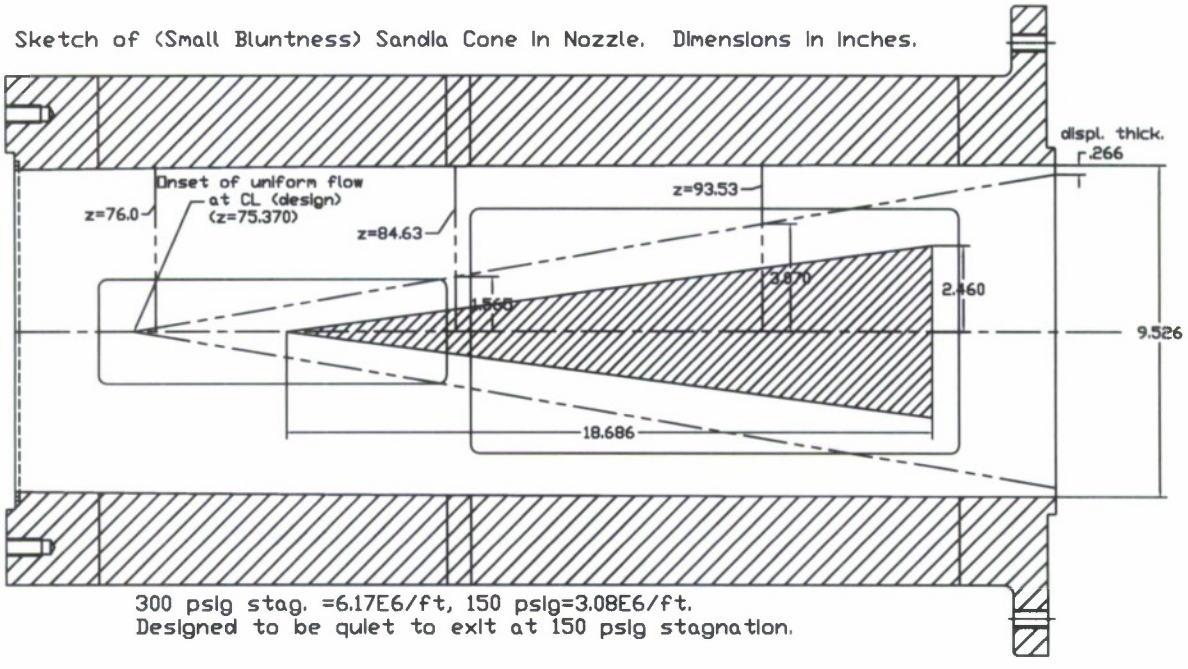

Figure 2: Schematic of Mach-6 Quiet Nozzle with Model

the diaphragm bursts, an expansion wave travels upstream through the test section into the driver tube. Since the flow remains quiet after the wave reflects from the contraction, sufficient vacuum can extend the useful runtime to many cycles of expansion-wave reflection, during which the pressure drops quasi-statically.

The contraction-wall boundary layer is bled off just upstream of the throat, beginning a fresh undisturbed boundary layer for the nozzle wall. At one time, the nozzle-throat bleed air could be ducted to two alternate locations. A fast valve is connected directly between the bleeds and the vacuum tank, allowing the bleed air to be dumped directly into the tank. In addition, the original plumbing connected the bleed air to the diffuser, to enable a simple and fast startup, if the jets of air into the diffuser do not cause a problem. If the bleed valves remain closed, the air entering the throat is disturbed by passing over the bleed slots, tripping the nozzle-wall boundary layer. Thus, these tunnels can run quiet and noisy at the same nominal operating condition, by opening or closing the bleed valves.

Unless otherwise specified, the initial stagnation temperature in the driver tube is set to $160°C$. The stagnation temperature drops about 10% during the run, as the air flows out of the driver tube [32]. The air in the nozzle at Mach 6 is supercooled, making Reynolds number computations dependent on the somewhat uncertain value of air viscosity at very low temperatures, but no evidence of condensation has been observed under these conditions [33], although further studies are needed.

Figure 2 shows the nozzle. Here, z is an axial coordinate whose origin is at the nozzle throat. The region of useful quiet flow lies between the characteristics marking the onset of uniform flow, and the characteristics marking the upstream boundary of acoustic radiation from the onset of turbulence in the nozzle-wall boundary layer. A 7.5-deg. sharp cone is

drawn on the figure. The rectangles are drawn on the nozzle at the location of window openings, all but one of which are presently filled with blank metal inserts. Images of the tunnel are available at `http://roger.ecn.purdue.edu/~ aae519/BAM6QT-Mach-6-tunnel/`, along with earlier papers and other documentation.

4 Achieving Quiet Flow at High Reynolds Number

During 2001-2005, the tunnel ran quiet only at very low Reynolds numbers. There were many possible causes for the low transition Reynolds number on the nozzle walls, as described in Ref. [23]. In 2005-2006, it was finally determined that the critical factor was a very small flaw in the contour of the bleed lip. The lip of the nickel throat was recut in 2006. Fig. 3 shows the old contour, using the solid symbols to depict measurements at four azimuthal angles. A small kink, about 0.001-in. high, is evident on the inner surface near $z = -0.98$. This kink apparently led to a small separation bubble upstream of the nozzle throat, which then induced early transition. It was not detected during the nozzle fabrication process, since the lip contour was not measured after machining, due to an excessive concern about scratching the finish. Following a Rutgers University design [18], the throat was recut to the shape shown by the open symbols, which should eliminate separation, according to an axisymmetric Navier-Stokes computation.

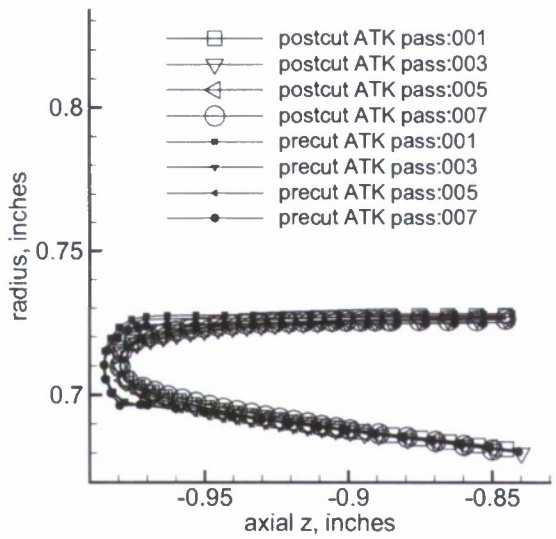

Figure 3: Measurements of Recut Geometry of Nickel Bleed Lip Compared to the Original Geometry

When the recut nozzle was first installed, it was still not quiet. After polishing, it took some time to blow dust out of the throat. However, beginning ca. Sept. 2006, the tunnel began to run quiet at higher Reynolds number, fairly reliably [5].

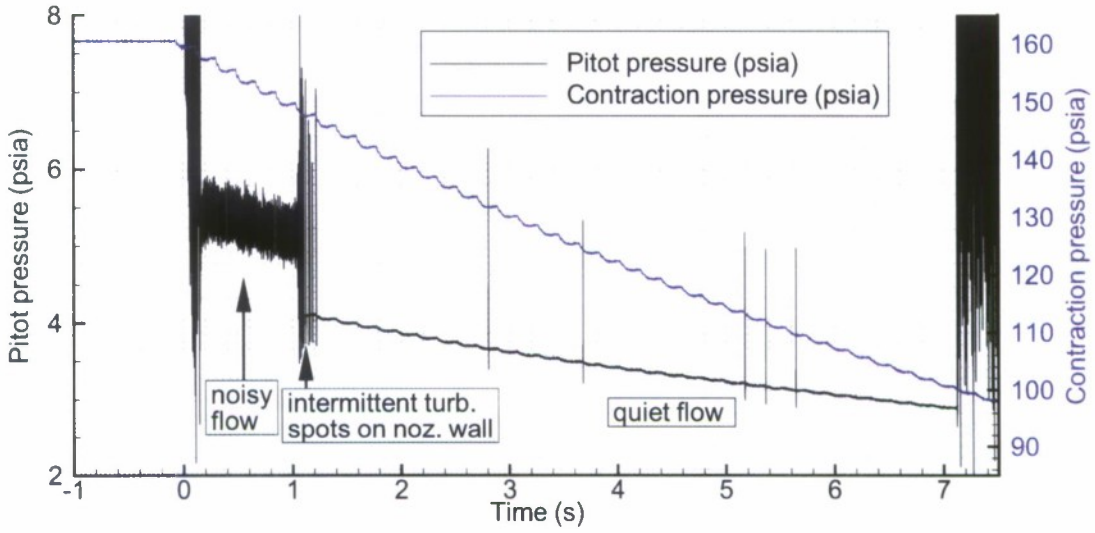

Figure 4: Pitot pressure for run becoming quiet at $p_t \simeq 146$ psia and $t \simeq 1.2$ sec

Three pieces of data were collected from each tunnel run on a Tektronix TDS7104 oscilloscope at 200kHz: the pressure in the contraction, the pitot pressure in the nozzle, and the high-frequency (ac) component of the pitot pressure. The pressure on the contraction wall, p_t, is measured near the entrance, where the Mach nunber is less than 0.01, so the pressure is very near stagnation pressure [33].

High-frequency Kulite pressure transducers (model XCQ-062-15A) are used to measure the pitot pressure. The stopped version of these transducers allows the test area to be pressurized to the high stagnation pressure without damaging the sensitive transducers. The DC pitot pressure is amplified by a factor of 100 before digitization, and the AC pitot pressure is high-pass filtered at about 840 Hz and amplified by an additional factor of 100 before digitization, using custom-built electronics based on INA103 instrumentation-amplifier integrated circuits. Hi-Res mode was used to increase resolution and decrease noise in the 8-bit scope, by averaging the sampled data on the fly before storing into memory at 11-12-bit resolution. The pressure transducers and associated electronics are calibrated quasi-statically using a Paroscientific quartz pressure transducer, by slowly filling the tunnel from vacuum.

Figure 4 is a typical oscilloscope trace, with the data converted from voltage to pressure using the calibrations. The oscilloscope records data for ten seconds and is triggered by the sudden drop in pitot pressure when the diaphragms burst. The first second of data is from before the trigger, and provides a baseline of electronic noise. At time $t \simeq 0.0$ s, the diaphragms burst and the run starts. Approximately 0.2 s is required to start up the Mach-6 flow. During this run, the tunnel runs at a conventionally high noise level until $t \simeq 1.0$ s. At $t \simeq 1.0$ s the boundary layer on the nozzle wall drops from turbulent to intermittent, becoming laminar and quiet at $t \simeq 1.2$ s. The contraction-wall pressure is shown in blue and referred to the right-hand axis. It drops from an initial value of 160 psia in stairsteps, each time the expansion wave reflects from the contraction. The contraction pressure at which the noise drops to quiet levels is about 146 psia. With the exception of

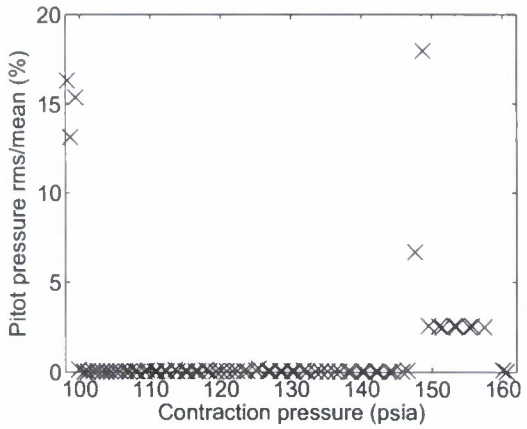

Figure 5: Typical Noise Level During a Run

five turbulent bursts between $t \simeq 2.8$ and 5.7 s, the tunnel is quiet until the run ends at $t \simeq 7.1$ s when the contraction-wall pressure has dropped 28% to about 105 psia. The mean pitot pressure drops when the flow becomes quiet, because the laminar nozzle-wall boundary layer is thinner, increasing the core flow Mach number to about 6.0 (quiet) from 5.8 (noisy). The pressure at which the nozzle drops quiet has nearly always been essentially independent of the time during the run at which this pressure is achieved [28, Sec. 6.2.2].

The pressure data is also used to calculate the tunnel noise level ($\tilde{p}/\bar{p}$). The noise level for the above run as a function of contraction pressure is shown in Figure 5. The noise is computed by breaking the run into 0.1-s intervals and calculating the root-mean-square ($\tilde{p}$) and mean ($\bar{p}$) pitot pressures over the segment. If the interval is quiet, the high-pass-filtered and amplified AC pitot pressure is used to find $\tilde{p}$; if not, the DC pitot pressure is used.

The noise level before the run is recorded as the point where the total pressure measured on the wall at the contraction entrance, p_t, is just less than 160 psia. As expected, the pre-run noise level is very small. The noise increases to 2.4 to 2.6% until $p_t = 149$ psia at which point the noise increases to near 18% during the series of turbulent bursts. When $p_t < 146$ psia the noise level decreases below 0.05%, except for the occasional turbulent spot (Figure 6). Near the beginning of quiet flow, the noise levels are about 0.02%; these are the lowest ever measured. The noise level increases dramatically when the run ends ($p_t < 100$ psia).

During the quiet portion of most runs, one or more short-duration pressure spikes would occur. These bursts all had a similar structure, such as the one in Figure 7. Less than 1.5 ms elapses between the onset of the spike and the pressure minimum, then the pressure increases back to the pre-spike level over the next 3.5 ms. The magnitude of the pressure spike is proportional to the stagnation pressure for the run and is greater than the pressure variation during noisy flow.

The burst is almost certainly caused by noise radiated from a turbulent spot on the nozzle wall. These bursts have often been seen in shadowgraphs (e.g, Fig. 1 in Ref. [34]) and in other quiet tunnels when operated at higher pressures just above laminar quiet levels [31, 35]. The pitot pressure trace at the time of the change from noisy to quiet flow shows

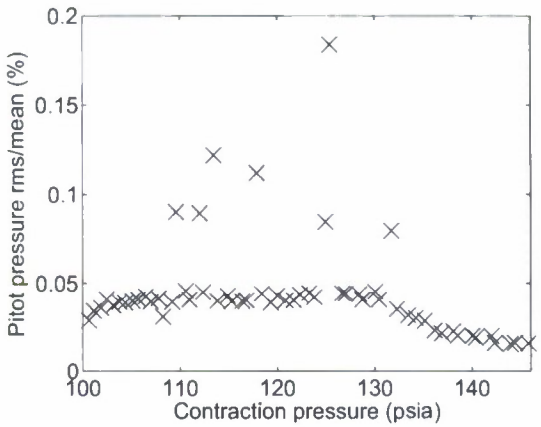

Figure 6: Typical Noise Level During Quiet Portion of Run

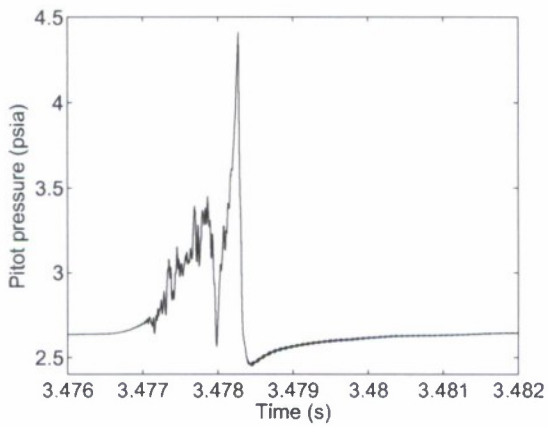

Figure 7: Turbulent burst

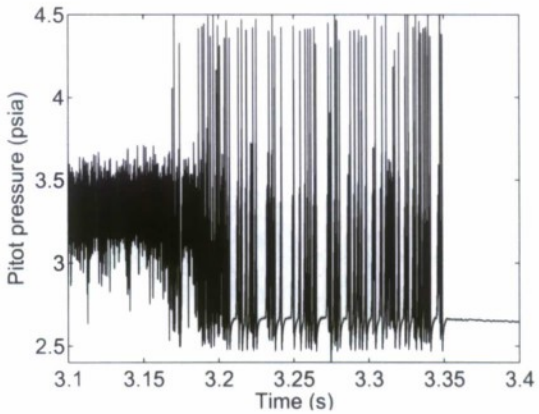

Figure 8: Turbulent bursts at onset of quiet flow

that a series of bursts occurs just before the flow becomes quiet (Figure 8). Regular noisy flow, on the other hand, produces irregular fluctuations and a histogram with a normally distributed band. These bursts are almost certainly the result of a turbulent nozzle-wall boundary layer dropping intermittently turbulent before it goes laminar, as the Reynolds number slowly falls.

5 Roughness-Induced Transition on the X-51A Forebody

5.1 Introduction

Ref. [25] reports experiments on the windward side of an X-51A model at an inviscid Mach number of 6.0 with an initial stagnation temperature of T_0=433 K (780°R) at 4.0° angle of attack; these are summarized here. The Purdue model is 20% scale and includes the forebody up to the engine inlet cowl. The model consists of a stainless steel nose section with an aluminum afterbody, as shown in Figure 9. The model includes a nylon 6/6 insert on both the windward and leeward sides. The nylon inserts were included to act as a thermal insulator layer for temperature sensitive paint (TSP).

For the purposes of the present experiments, TSP is fairly quantitative in temperature. Efforts are underway to make it reliably quantitative in temperature and heat transfer. At present, the uncertainties associated with this method are too large for accurate quantitative results. However, this technique has demonstrated consistently that temperature scales monotonically with intensity. To reliably measure the location of transition, precise temperatures are not needed. The 'y' coordinates reported in some figures correspond to spanwise location, with y=0 being the centerline.

A smooth strip and two trip strips with different roughnesses were used in the model at a streamwise location of x=6.30 cm (2.48 in.). One of the trip strips is composed of ramp-shaped roughness elements while the other has diamond-shaped trips. The roughnesses have the same shape as those used by Berry et al. on the Hyper-X model [36].

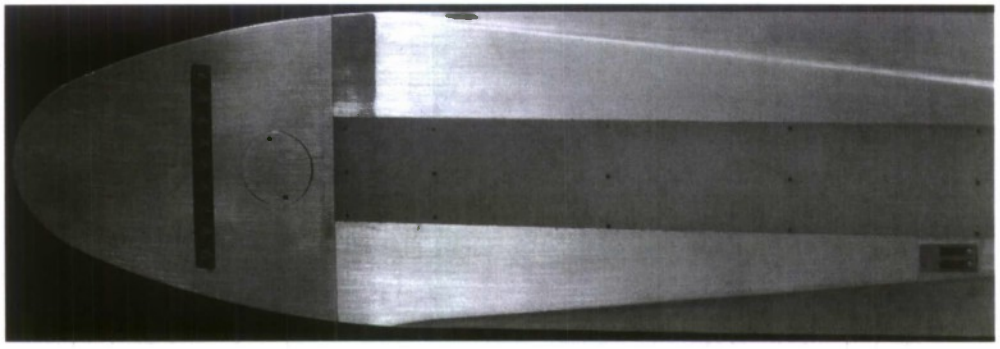

Figure 9: Photograph of windward side of model

A photograph of the three strips used in the Purdue model can be seen in Figure 10. Here, the flow is from top to bottom. The upstream edge of the ramp roughnesses are at the same height as the model surface. Moving downstream, they rise up above the model surface and also become increasingly narrow. At the downstream edge, the ramps have a maximum height of 0.076 cm (0.030 in.).

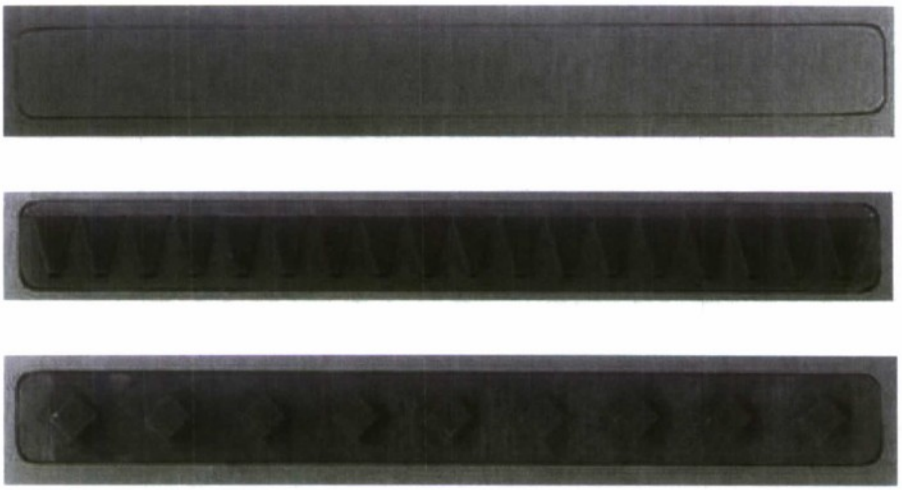

Figure 10: Trip inserts for model

5.2 Effect of Tunnel Noise

Runs were made with an initial stagnation pressure of 655 kPa (95 psia) with all three inserts in the model. The tunnel was run under noisy and quiet conditions to assess the effects of noise on natural and roughness-influenced transition.

When the tunnel is run noisy (with the throat bleed suction turned off), the total mass flux out of the driver tube decreases by about 38% from the bleeds-open case, the nozzle-wall boundary layer becomes turbulent, the flow becomes noisy, and the mean Mach number

decreases from about 6.0 to about 5.8 due to the difference in the displacement thicknesses between the laminar and turbulent boundary layers. This, in turn, means that the freestream Reynolds-number drop with time is less with the bleeds closed than with the bleeds open. When comparing data taken under noisy and quiet conditions, a choice needed to be made regarding whether to compare data at the same freestream Reynolds number or to compare data taken at the same time after the start of the run. The problem with comparing data at the same Reynolds number is that these data were taken at significantly different times during the run. It has been observed that over the course of a run, the mean temperature of the nylon increases. It was therefore decided to compare data taken at similar times into a run. This leads to a small variation in Reynolds numbers when comparing these data. The difference in the Mach number between quiet and noisy tunnel runs also leads to a difference in Reynolds number, even if stagnation conditions are the same.

5.2.1 Smooth Insert

Figure 11 shows the surface temperature distributions with the smooth insert under quiet and noisy conditions, at freestream Reynolds numbers of 6.59 and 7.38×10^6/m (2.01 and 2.25×10^6/ft), respectively. The freestream Reynolds numbers are calculated using an isentropic theory for Ludweig tubes [37]. This theory takes into account the falling stagnation pressure and temperature inherent in a blow-down facility. The stagnation temperatures (T_0) and pressures (P_0) were T_0=418 K (752°R) and P_0=586 kPa (85 psia) with the tunnel running quietly. With the noisy tunnel, T_0=424 K (763°R) and P_0=621 kPa (90 psia). The dashed red line indicates the compression corner. Figure 12 shows the streamwise temperature distribution on the centerline. The gaps in the data are due to the registration marks on the model surface. The compression corner is marked by the dashed black line.

Under quiet conditions, both the TSP image and the centerline temperature distribution show that the temperature increases downstream of the compression corner followed by a nearly monotonic decrease for the rest of the extent of image. This strongly suggests a laminar boundary layer over the entire length of the nylon insert. Faint streaks are also visible in the TSP image. They are most likely due to the presence of streamwise vortices near the model surface.

The results for the noisy tunnel case are very different and clearly discernible in Figure 11. For the noisy case, after the expected rise at the corner, the temperature rises at an increased rate starting at about x=17.8 cm (7.0 in.), peaks at about x=26.8 cm (10.6 in.), and then decreases to the end of the model. This sudden rise in surface temperature is a strong indicator of transition; this was confirmed by measurements with hot wires and hot films. From Figure 12, it is reasonable to assume that centerline transition onset takes place at around x=14.0 cm (5.5 in.). This is where the centerline surface temperature under noisy conditions significantly departs from that under quiet conditions.

It is difficult to know whether the distance from the leading edge, distance from the strip, or distance from the compression corner is the appropriate length parameter for transition. For the smooth-walled case, the distance from the nose is the most important length. Transition Reynolds numbers based on freestream conditions will be reported. It would be better to calculate the Reynolds number based on edge conditions, but at present, this is not feasible.

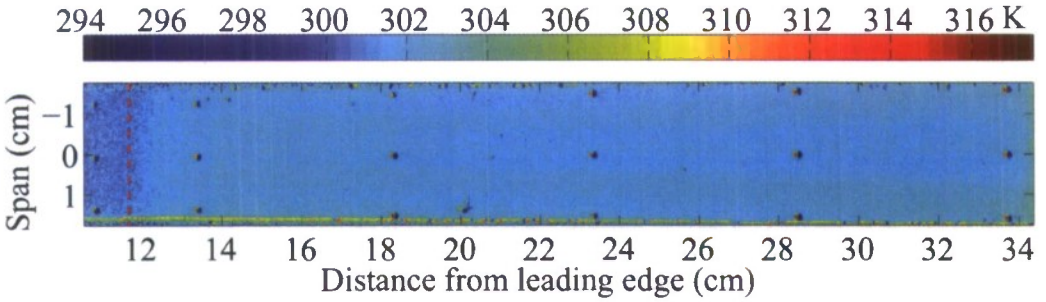

(a) Surface temperature for quiet flow, smooth insert, Re=6.59×10^6/m (2.01×10^6/ft)

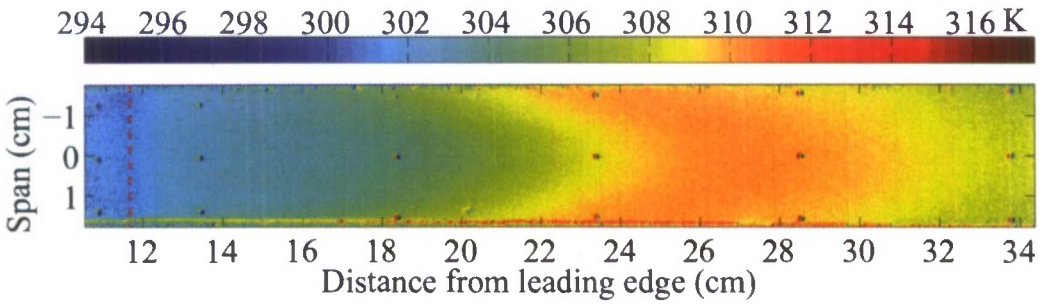

(b) Surface temperature for noisy flow, smooth insert, Re=7.38×10^6/m (2.25×10^6/ft)

Figure 11: Surface temperature (K) under quiet and noisy conditions with smooth trip insert for Re=6.59 and 7.38×10^6/m (2.01 and 2.25×10^6/ft)

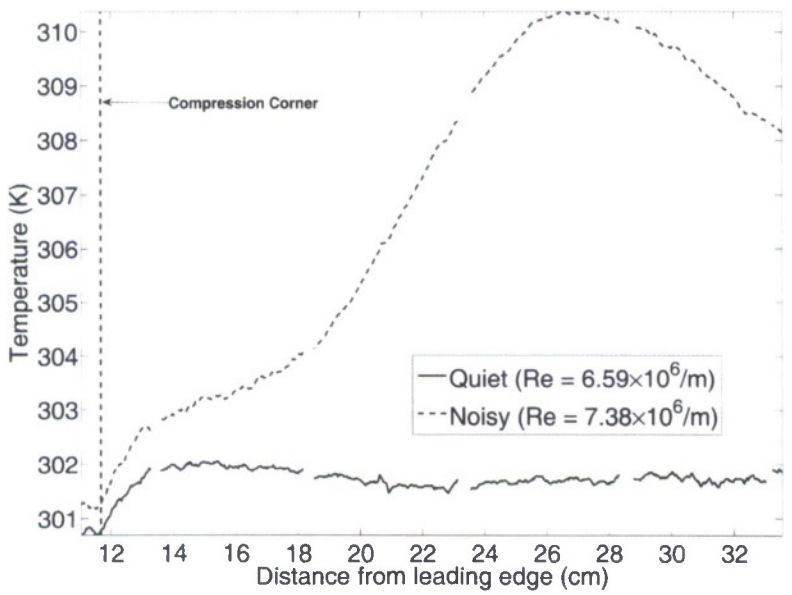

Figure 12: Centerline temperature for smooth insert, quiet and noisy flow, Re=6.59 and 7.38×10^6/m (2.01 and 2.25×10^6/ft)

Reducing freestream noise levels from conventional to quiet levels caused the transition Reynolds number based on distance from the nose to transition onset to increase by a factor of at least 2.2 from 1.03×10^6 to greater than 2.27×10^6. The actual increase cannot be determined since the flow is laminar past the end of the model under quiet conditions at the maximum quiet Reynolds number.

The vortices observed under quiet flow suggest that the dominant natural, untripped transition mechanism may not be the amplification and breakdown of first or second mode waves. Spanwise spreading of the streamwise vortices indicates outward directed cross flow. Natural transition may be dominated by vorticity from the leading-edge or three-dimensional crossflow. Transition may also be due to some complex coupling of leading edge vorticity, crossflow, and first or second mode waves with a shear layer instability above a separation bubble at the corner [34].

5.2.2 Ramp Roughness Insert

Figure 13 shows the surface temperature distribution with the ramp roughness strip under quiet and noisy conditions for Re=6.63 and 7.45×10^6/m (2.02 and 2.27×10^6/ft), respectively. For the quiet case, T_0=418 K (752°R) and P_0=586 kPa (85 psia) while under noisy conditions T_0=424 K (763°R) and P_0=627 kPa (91 psia). There are clearly significant temperature changes in both the streamwise and spanwise directions. No single cut of temperature can completely capture these variations.

Figure 14 shows the streamwise centerline temperature as well as the streamwise temperature along the line y=-0.2 cm for both noisy and quiet cases. The significant difference between quiet and noisy flow is immediately evident from the images. Along the centerline for the quiet case, the temperature increases by about 6 K (11°R) from the compression corner to x=15.2 cm (6 in). This is significantly higher heating than for the smooth insert case shown in Figure 12, which increased by only about 1 K (2°R) downstream of the corner. This region of high heating is followed by a decrease in temperature from x=15.5 cm (6.1 in.) to x=21.6 cm (8.5 in.). At this point, the temperature increases sharply to a second peak at x=25.7 cm (10.1 in.) followed by a gradual decrease to the end of the model.

It appears that the first temperature rise is due to the combination of compression heating as well as heating due to the laminar vortices near the model surface that are shed from the trip elements. The streamwise streaks in Figure 13a are most likely due to these vortices.

The streamwise temperature decrease after the first peak is attributed to the thickening laminar boundary layer. The second temperature increase, starting at around x=21.6 cm (8.5 in.), is due to the onset of transition, as was confirmed by hot-wire measurements. Schneider [34] states that the maximum surface temperature generally corresponds to the middle of transition. Thus, at x=26.7 cm (10.5 in.), it seems that the boundary layer is well on its way to being fully turbulent with the subsequent temperature decrease due to the thickening turbulent boundary layer.

Under conventional noise levels, this type of behavior is not seen. Rather, there is a sharp rise in temperature from the corner, x=11.7 cm, (4.6 in.) to x=14.0 cm (5.5 in.). This high-temperature peak is then followed by a nearly monotonic decrease to the end of the model. The sudden rise in surface temperature and subsequent decrease suggests that the boundary layer transitions just downstream of the corner. This inference was confirmed by

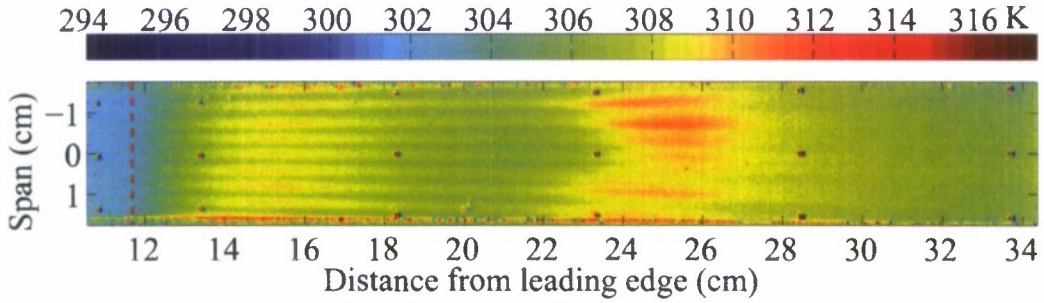

(a) Surface temperature for quiet flow, ramp trips, Re=6.63×10^6/m (2.02×10^6/ft)

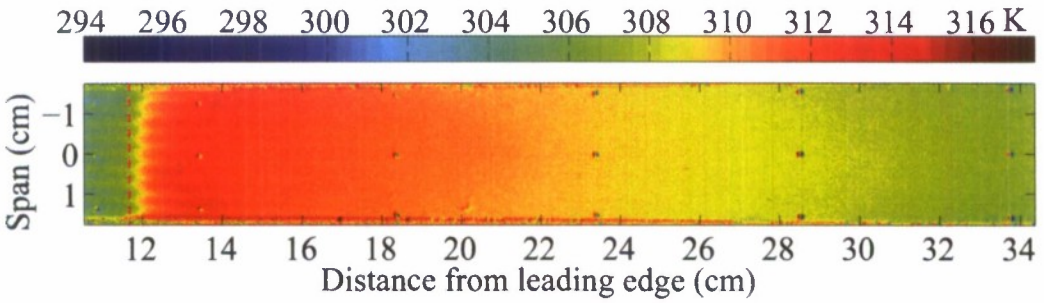

(b) Surface temperature for noisy flow, ramp trips, Re=7.45×10^6/m (2.27×10^6/ft)

Figure 13: Surface temperature (K) distribution with ramp trips under quiet and noisy conditions

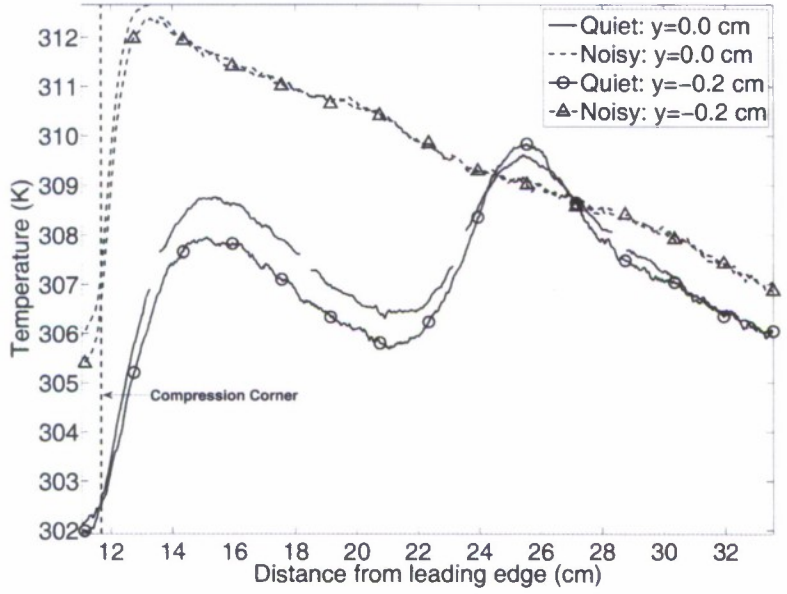

Figure 14: Streamwise temperature for centerline and y=-0.2 cm (-0.08 in.) for ramp trips, quiet and noisy flow, Re=6.63 and 7.45×10^6/m (2.02 and 2.27×10^6/ft)

hot-wire measurements.

5.3 Conclusions

The effect of tunnel noise on natural and roughness-dominated transition was clearly seen on the 20%-scale X-51A forebody model in the BAM6QT. On the smooth model, no transition was observed in the TSP under quiet flow at Re=6.60×10^6/m (2.01×10^6/ft), giving a transition Reynolds number based on distance from the leading edge of at least 2.27×10^6. When the tunnel was noisy, however, a clear transition front was seen by about x=17.8 cm (7.0 in.) with an associated transition Reynolds number of 1.03×10^6. Reducing freestream noise from conventional to quiet levels increased the transition Reynolds number based on freestream conditions and length from the nose by a factor of at least 2.2.

With the ramp roughness strip in the model under quiet conditions at Re=5.87×10^6/m (1.79×10^6/ft), an initial temperature rise downstream of the compression corner was observed and attributed to laminar vortex heating. Further downstream, at about x=21.0 cm (8.3 in.), the onset of transition was observed with TSP and confirmed by hot-wire spectra. Under noisy conditions at Re=7.45×10^6/m (2.27×10^6/ft), the ramp roughnesses caused transition almost immediately downstream of the corner. Reducing freestream noise from conventional to quiet levels increased the transition Reynolds number by a factor of 2.4 where the length parameter is the distance from the strip.

6 Roughness-Induced Transition on a Slender Cone

These X-51A measurements were surprising, even to the present author [22], since tunnel noise had a marked effect even for large roughness elements which were nearly 'effective'. This led to a strong interest in similar measurements on other geometries. There was particular interest in measuring on a public-release geometry where the wake of the roughness could be more easily computed. Ref. [11] reports the effect of tunnel noise on roughness-induced transition for a slender cone to be flown as HIFiRE-1. The HIFiRE model is a seven-degree half-angle nylon cone with a 4-in. base diameter. This cone is a 36.9% model of the forecone of the HIFiRE vehicle with the exception of the nose radius. A stainless steel 0.047-in. radius nose was used. This radius was chosen to match the size of the full-vehicle models tested at NASA LaRC. The nylon portion stretches axially from 5.77 in. to 15.95 in. This section was painted with temperature-sensitive paint and used to visualize surface temperature. The nylon acts as an insulator and increases the temperature variations seen at the surface. Reference marks were applied for image alignment on the nylon frustrum. Reference marks are located on the windward ray and at $\pm$ 35 and 70 degrees. The marks are located 1 in. from the base of the model and spaced every 1.5 in. along the nylon portion of the cone.

A single roughness element was placed on the model for each run as shown in Figure 15b. Roughness elements were 0.05 by 0.05-in. squares, sized to match NASA LaRC's wind tunnel test trips. The trips were made from plastic shims and glued to the model. Each trip was placed with a corner in line with the free stream and on the windward ray for all measurements at angle of attack. Johnson computed the mean flow over the model at estimated tunnel conditions. The displacement thickness at the roughness location was used

to scale the roughness height from the NASA Langley tests. A trip height of 0.014 in. was thought to match NASA LaRC's trip height of $3.2\delta^*$, though later computations at actual run conditions showed this trip height corresponded to $2.2\delta^*$, and a trip height of 0.021 in. corresponded to the desired height of $3.2\delta^*$. The trip was placed at an axial distance of 5.1 in. to equal the Re_{xk} for NASA LaRC at 135 psia, which at the time was the maximum pressure at which the BAM6QT was quiet.

The 0.014-in. roughness height did not cause transition at zero angle of attack under quiet flow. In order to find an effective trip, higher roughness heights were then tested. Heights tested at zero angle of attack were 0.014, 0.018, 0.021, and 0.028 in, which corresponded to $2.2\delta^* - 4.3\delta^*$ per computations. At 6° angle of attack, the 0.014-in. high trip did cause transition when placed on the windward ray. Smaller trip heights of 0.004, 0.007, 0.011 in. were tested to find the limit of the trip effectiveness. A larger trip height of 0.028 in. was also tested. These heights corresponded to $1.1\delta^* - 7.7\delta^*$.

A typical model installation at zero angle of attack is shown in Figure 15. A number of variables were changed during tests. The model was tested at zero and six degrees angle of attack. The trip height was varied between 0.004 and 0.028 in. Most tests were run at 433 K initial stagnation temperature and at the maximum quiet pressure of the tunnel. The maximum initial stagnation pressure for quiet flow was 135 psia at the time of testing. This corresponded to a unit Reynolds number of 3.0×10^6/ft. A few runs were conducted at 5.6×10^6/ft under noisy flow (initial stagnation pressure of 255 psia) in order to match NASA LaRC test conditions.

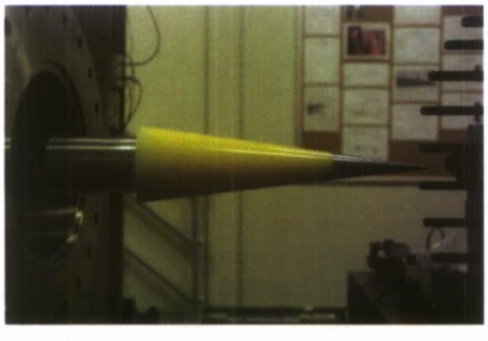

(a) Model setup in the BAM6QT

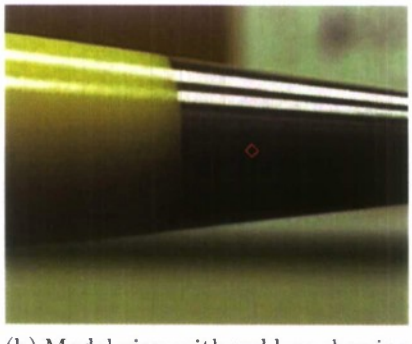

(b) Model view with red box showing location of roughness element

Figure 15: Model setup for testing in the BAM6QT, prior to installation of new sting support section in December 2007

6.1 Results

A parametric study of trip height was conducted at both zero and six degrees angle of attack, but only the zero AOA data is shown here. Figure 16 shows TSP images for the model under noisy and quiet flow at zero angle of attack, for increasing trip heights. Flow conditions for each image as well as the measured transition locations at 0° AoA are found in Table 1. In all cases, two straight streaks can be seen in the wake of the roughness element. Several inches downstream of the trip, the wake spreads and a turbulent wedge appears. Transition

is inferred at this location, when a rise is also seen in the centerline surface temperature. Figure 17 plots the roughness Reynolds number for each trip height against the transition onset location under both noisy and quiet flow. The smallest trip height corresponds to the smallest roughness Reynolds number. A noticeable difference between the noisy and quiet flow conditions can be seen. The same trip heights that caused transition on the model under noisy flow did not necessarily cause transition on the model in quiet flow. When transition did occur, it was delayed. The ratio of transition Reynolds numbers under noisy and quiet flow at 0° AoA can be seen in Table 2. An increase of up to 6.4 times the noisy transition Reynolds number when referenced to the trip location was observed under quiet flow. When referenced to the nose, the transition Reynolds number increased by factors of up to 2.2.

Under noisy flow, it is interesting to note that the transition location behind the roughness element does not noticeably change with increasing trip height, beyond a point. The smallest roughness height of 0.014 in. is not fully effective at 0° AoA. However, the 0.018-in. trip as well as the 0.021 and 0.028-in. trips cause transition at approximately the same location on the model. This indicates that a 0.018-in. trip may be fully effective under noisy flow. Under quiet flow, the 0.014-in. high trip generated a pair of vortices, but the flow remains laminar to the end of the cone. The 0.018-in. high trip also generated two streaks in its wake, and transition begins just before the end of the model. The 0.021 and 0.028-in. high trips both caused transition downstream of the trip, but the transition location does not change significantly between these two trip heights (Figure 17). This may indicate that the effective transition height for quiet flow conditions has nearly been reached. It would be interesting to test higher trips to see if the transition location can be moved further forward under both noisy and quiet flow conditions and to confirm when an effective trip height has been reached.

For a less-than-effective trip under quiet flow, there was a significant difference between quiet and noisy flow transition locations. For example, a trip height of 0.018 in. (less-than-effective under quiet flow) delayed transition by 6.4 times when referenced to the trip location and 2.2 times when referenced to the nose. Berry and Horvath [38] recently hypothesized that tunnel noise would "have an effect on the transition process only when the trips are less than fully effective." The present author had also expressed a similar hypothesis [22]. However, a delay in the transition location was still seen with effective trips under quiet flow when compared to noisy flow results. For an effective trip under both quiet and noisy flow, the ratio of the quiet to noisy transition Reynolds number was 2.1 when referenced to the trip location and 1.3 when referenced to the nose. The difference in transition location between quiet and noisy flow conditions is significantly reduced when effective trips are used, but quiet flow still delays the transition location for an effective trip. A similar result was seen for experiments at angle of attack. It seems that higher levels of tunnel noise cause larger initial amplitudes for the instabilities in the roughness wake, and thus earlier transition.

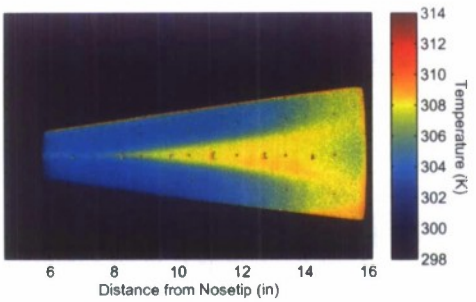

(a) k=0.014 in.

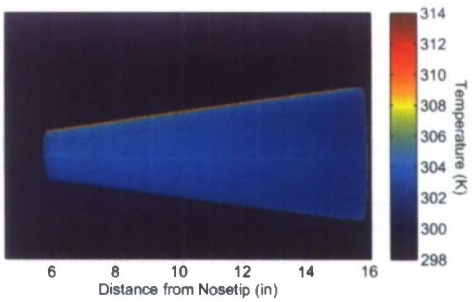

(b) k=0.014 in.

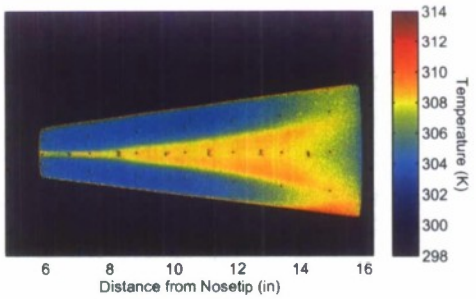

(c) k=0.018 in.

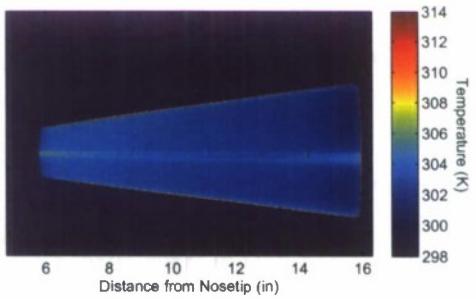

(d) k=0.018 in.

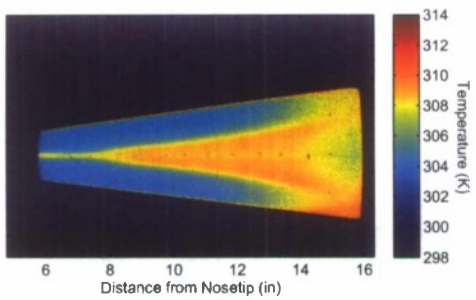

(e) k=0.021 in.

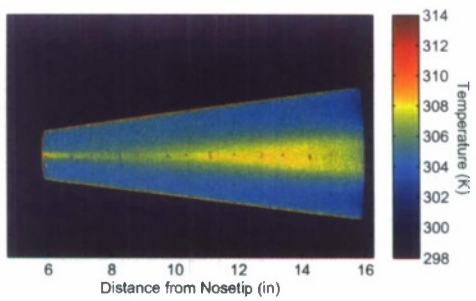

(f) k=0.021 in.

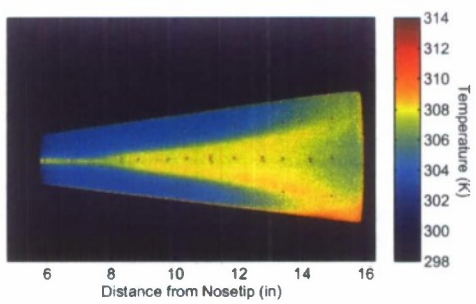

(g) k=0.028 in.

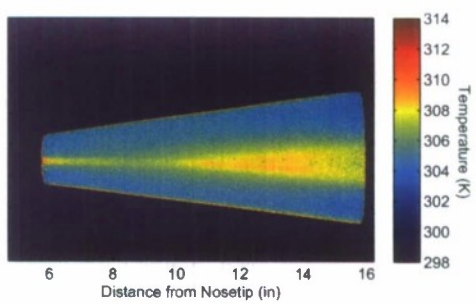

(h) k=0.028 in.

Figure 16: Effect of trip height under noisy and quiet flow at 0° AoA. Noisy flow is shown in left column and quiet flow in right column.

noisy/quiet	k (in.)	P_0 (psia)	T_0 (K)	t (s)	Re/ft $\times 10^{-6}$	x_{tr} (in)
noisy	0.014	129	427	1.1	2.9	7.3
noisy	0.018	129	426	1.2	3.0	6.5
noisy	0.021	128	426	1.3	2.9	6.8
noisy	0.028	131	427	1.0	3.0	6.7
quiet	0.014	128	425	0.89	2.9	n/a
quiet	0.018	125	423	1.2	2.9	14
quiet	0.021	127	425	1.0	2.9	8.5
quiet	0.028	126	424	1.1	2.9	8.5

Table 1: Image conditions and transition location for various trip heights at 0° AoA. Trip located at 5.1 in.

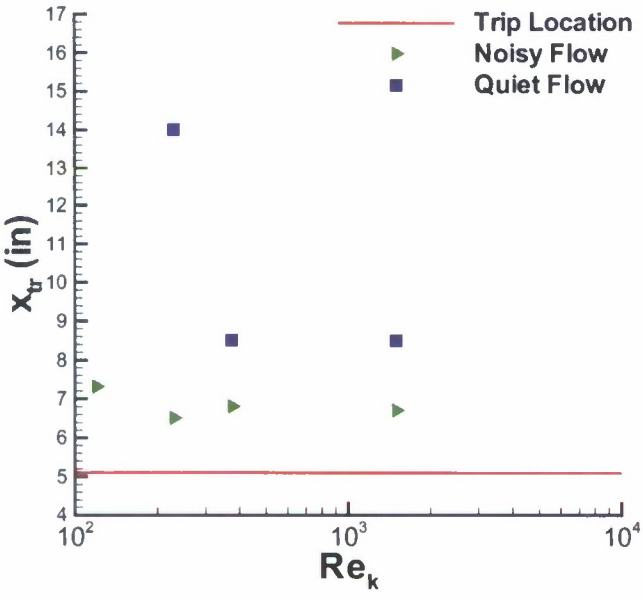

Figure 17: Effect of trip Reynolds number on transition location at 0° AoA

k (in.)	k/δ^*	Re_k	Delay Factor Referenced from Trip	Delay Factor Referenced from Nose
0	0	0	> 2.2	> 1.6
0.014	2.2	120	> 5.0	> 2.2
0.018	2.8	230	6.4	2.2
0.021	3.2	380	2.0	1.3
0.028	4.3	1500	2.1	1.3

Table 2: Quiet to noisy ratio of transition Reynolds number referenced to both the trip location and nose at 0° AoA

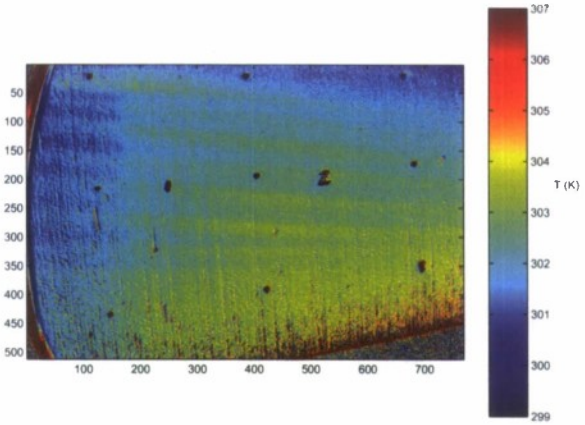

Figure 18: Crossflow Vortices on Cone at AOA in Quiet Flow at $Re_\infty = 3 \times 10^6$/ft.

7 Transition in 3D Flow Induced by Stationary Crossflow

7.1 Cone at Angle of Attack

Crossflow vortices have been observed on a cone at 6-deg. angle of attack under quiet and noisy conditions [5, 27]. For the measurements shown here, the freestream unit Reynolds number was 3 million/ft. The sharp cone had a base radius of 2.0 inches and a half-angle of 7.0 deg. The frustum was fabricated from nylon 6/6 and painted with a temperature-sensitive paint consisting of Ru(bpy) luminophore molecules in DuPont ChromaClear paint. The paint was calibrated for temperature. The aluminum nosetip had a tip radius of 0.002 in. and was not roughened. The model was viewed through the downstream 5-in.-dia. opening of the dual porthole window in the nozzle [39]. A Photometrics SenSysB scientific-grade CCD camera was used to acquire the images. The paint was excited with 464-nm light from a 4-inch diameter ISSI LM4 blue LED array. A grid of rub-on microdots was applied to the frustum as reference marks. The stagnation temperature was $160°C$.

Figure 18 shows the temperature distribution on the downstream portion of the yawed cone in quiet flow. Several crossflow vortices can be seen. The boundary layer is laminar. The vortices correspond to the vortices seen in the oil flow images shown in Figures 16 and 18 of Ref. [40], which were taken under noisy conditions. The vortices increase the temperature of the cone surface very little over the initial 300 K. The low heat transfer under the thick laminar boundary layer on the downstream portion of the cone contributes to the noisiness of the image. A new coat of TSP would probably help to increase the signal-to-noise ratio.

Figure 19 shows the temperature distribution for the yawed sharp cone under noisy conditions, with the tunnel bleed valves closed, at the same tunnel pressure and temperature, and the same yaw angle. Leeside-forward transition is evident through the higher temperature (and corresponding higher heat transfer) on this section of the cone. Since this relatively small image was acquired through the 5-inch porthole window, the leeside-forward transition

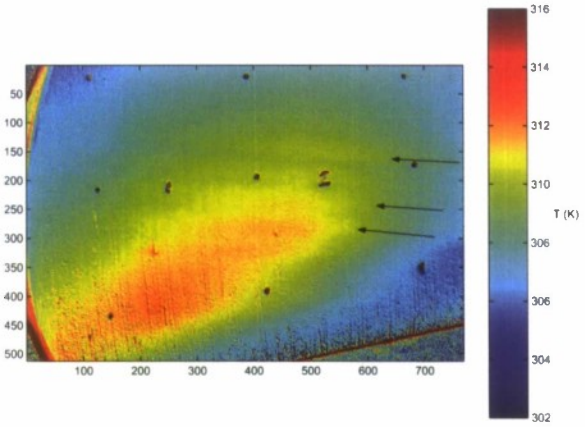

Figure 19: Crossflow Vortices on Cone at AOA in Noisy Flow at $Re_\infty = 3 \times 10^6$/ft.

is not as evident as in full-model images acquired earlier through the large 7x14-inch rectangular window. Transition in the noisy flow appears to occur near the region where vortices are first seen in quiet flow.

The black arrows in Figure 19 point to streaks of slightly higher heat transfer that seem to correspond to the crossflow vortices seen in Figure 18. This could mean that the vortices maintain organization some distance into the turbulent boundary layer; they are not yet broken apart by the turbulence. This might be why vortices were observed on this downstream section of the cone under noisy conditions in the oil-flow images of Ref. [40]. The small, random turbulent eddies may not disturb the oil as much as the organized motion of the vortices.

Thus, there seems to be a large effect of tunnel noise on transition induced by the stationary crossflow instability. Although the stationary crossflow waves probably originate from roughness on the cone surface, it seems that the tunnel noise causes the waves to break down to turbulence much earlier, perhaps when they are of much smaller amplitude. This is not surprising, since unsteady secondary instabilities developing on the stationary crossflow waves often cause transition on swept wings [41]. Such unsteady secondary instabilities would begin with much higher amplitudes when the freestream noise is much higher.

These were the first hypersonic measurements of the effect of tunnel noise on crossflow instability. The role of the crossflow instability in the transition process was investigated further for Erick Swanson's Ph.D. research [27]. Measurements similar to Figs. 18 and 19 were obtained with a 0.06-in. nose radius. Controlled roughness was also applied to the cone, in attempts to generate controlled vortices, following the work of Saric's group at low speed [42]. However, the controlled-roughness work has met with limited success, to date.

7.2 HIFiRE-5

Experiments have been conducted on a model of the HIFiRE-5 2:1 elliptic cone (Figure 20). The geometry was designed by Roger Kimmel et al. at AFRL as part of the HIFiRE-5

program [43]. The 0.381-scale model was designed at Purdue and fabricated by Tri-Models, Inc. It has a steel nosetip and aluminum frustum. It can accommodate thermocouples, heat transfer gages, and fast-response pressure sensors along its centerline (semi-minor axis). Temperature-sensitive paint (TSP) is the only instrumentation that has been employed thus far. The first application of the spray-on insulator between the TSP and the frustum resulted in a rough finish that resembles an orange peel.

Figure 20: 0.381-scale HIFiRE-5 forebody model with orange peel finish TSP

Experiments were done with the substandard paint job to investigate the effect of the distributed roughness on transition; these experiments are providing interesting preliminary data, indicating a significant effect of unknown properties of the roughness. Quiet and noisy flow runs were made at 0 and 4-deg. AOA for Re from 0.9 to 3.0 $\times$ 10^6 /ft. Figure 21 shows TSP data from a quiet run for $\alpha = 0$, $Re = 2.6 \times 10^6$ /ft. The contour levels give the ratio of paint intensity I_{ref}/I, where I_{ref} is the intensity with the flow off and I is with the flow on. Higher I_{ref}/I corresponds to higher surface temperature, although the TSP is uncalibrated. This surface temperature increases monotonically with the heat transfer rate, although quantitative determination of the heat transfer is not yet accurate or reliable. This run is interesting because it exhibits both centerline transition and what appears to be crossflow transition between the centerline and leading edges. Hot streaks, presumed to be crossflow vortices, increase in temperature and width as the boundary layer transitions.

The model was subsequently repainted and the tests were repeated. The new paint job is smoother than the first one, but is rough near the leading edges. Under the same flow conditions, streamwise streaks are visible but they do not breakdown to turbulence before the end of the model (Figure 22). It is unclear if these streaks are crossflow vortices or result from the flawed paint job near the leading edges. Future tests are planned with improved paint to better estimate smooth-wall transition. Similar experiments are also to be carried out with a circular cone at angle of attack. The goal is to determine the way in which roughness affects transition induced by stationary crossflow vortices, again following the work of Saric's group on swept wings at low speed [42].

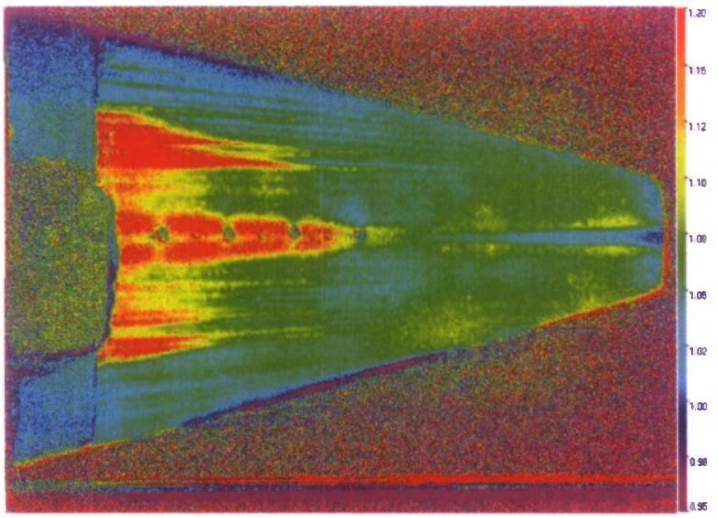

Figure 21: Orange peel finish, quiet flow, $M = 6.0$, $Re = 2.6 \times 10^6$ /ft., $T_0 = 425$ K, $p_0 = 114$ psia, $\alpha = 0$

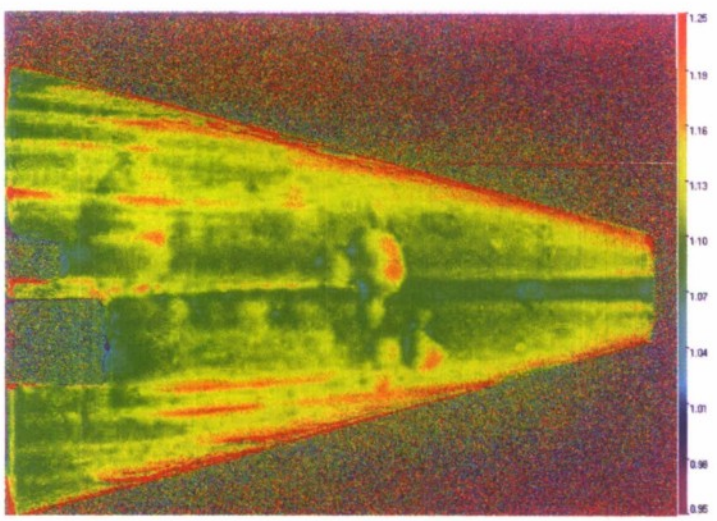

Figure 22: Rough leading edges, quiet flow, $M = 6.0$, $Re = 2.6 \times 10^6$ /ft., $T_0 = 425$ K, $p_0 = 114$ psia, $\alpha = 0$

8 Measurements of Second-Mode Instability Waves Using Robust Surface Sensors

Although the Purdue and Texas A&M quiet tunnels simulate the low noise levels of hypersonic flight, they can do so only in low-enthalpy flow at Mach 6. No single ground facility can simulate all aspects of hypervelocity flight at high enthalpy. Transition measurements are thus of limited value, since improved prediction methods must approximate the instability mechanisms that lead to transition. These instabilities must be measured with the help of controlled perturbations, to help develop and validate the computational models.

Hot wires have traditionally been used to measure both traveling and stationary instabilities, especially at low speeds. Rufer used hot wires to measure the second-mode waves on a cone at zero angle of attack under noisy flow in the Purdue tunnel [4]. However, hot wires are intrusive, fragile and difficult to work with at high speeds. Robust high-frequency sensors capable of measuring instability waves would improve efficiency, and also enable ground experiments in the many facilities that are too harsh to permit use of hot wires. Nonintrusive techniques for measuring the waves would also enable wave-growth measurements using multiple sensors in a single tunnel run, a characteristic that is increasingly important for higher-energy tunnels that are more expensive to operate. In the last few years, two promising new flush-surface sensors have appeared and are beginning to produce results.

8.1 Measurement of Second-Mode Waves Using Fast Quartz Pressure Sensors

Following work by Fujii in Japan [44], Estorf et al. measured second-mode waves on a 7-deg. sharp cone in the Mach-6 Ludwieg tubes at Purdue and Braunschweig [8]. Figure 23 shows samples of pressure-fluctuation spectra at three consecutive sensors. The data in Figure 23a were collected at Purdue under quiet flow at a 89.3 psia driver-tube pressure. This was the lower limit of the pressure range where the second mode could be detected under quiet flow. Note that the amplitude of the fluctuations at that pressure is close to the limit of the available resolution (10^{-6} psi at 16 bit). Therefore the signal-to-noise ratio is very small and only the large number of averaged FFTs (8000 windows) brings out the 2nd mode peaks. Also note that the resolution of the pressure sensors is specified as 10^{-3} psi in the manufacturer's datasheet. Moreover the diameter of the sensing surface (3.18 mm) is larger than half the wavelength of the second-mode waves, where half the wavelength can be approximated by the boundary layer thickness of 2 mm. For these reasons, the absolute amplitudes given in the figure are questionable and have to be understood as some uncertain nonlinear function of the actual fluctuation amplitude at a certain frequency. The spectrum shown in Fig. 23b was measured at 110.6 psia driver-tube pressure and shows a second-mode amplitude that is an order of magnitude higher. The figure also shows integrated amplification rates from the linear stability calculation of *case1* based on the similarity solution. The calculated amplitudes are scaled to match the amplitude at the second sensor position. The measured amplification seems to be somewhat higher than the calculation. The calculated frequencies are lower than those measured, by about 8 kHz. This frequency shift may be due to a small angle of attack. However, the bandwidth of amplified frequencies is almost the same in the

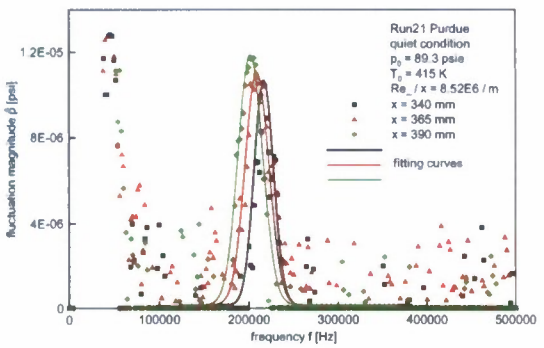

(a) measurement and curve fit

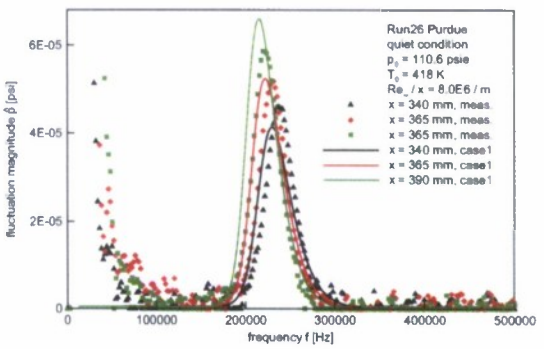

(b) measurement and calculation

Figure 23: Spectra of pressure fluctuations measured in quiet Mach-6 flow

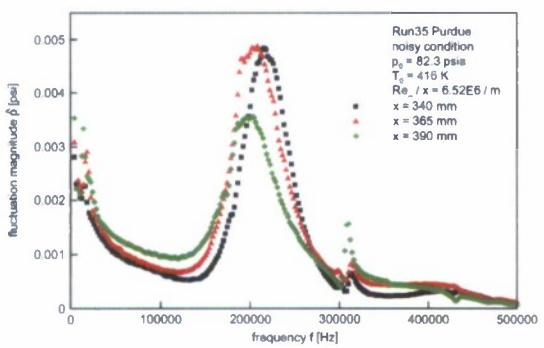

(a) noisy condition Purdue

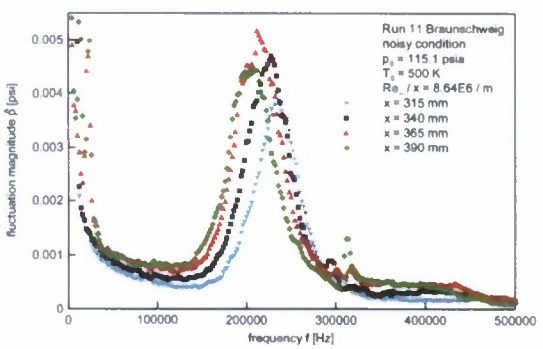

(b) noisy condition Braunschweig

Figure 24: Spectra of pressure fluctuations measured in noisy Mach-5.8 flow

measurement and the calculation.

Figure 24 shows spectra in noisy flow measured at the same Reynolds number as in Fig. 23a, at similar stagnation conditions. In noisy flow the measured pressure amplitudes are about 450 times higher. The second-mode peaks in noisy flow are much broader and first harmonics can be detected. The small peak at about 310 kHz is thought to be an effect of the sensors although this is far below the resonant frequency claimed by the manufacturer. At this Reynolds number in noisy flow the boundary layer appears to be transitional, since the second mode amplitude growth stagnates and reverses between the second and third streamwise sensor. Note that the results in the Braunschweig tunnel show the same behavior at nearly the same Reynolds number and wave amplitude (Fig. 24b). Since no data was collected at Purdue at lower unit Reynolds numbers than shown in Fig. 24, we can compare data at the noisy condition only, as described with the Braunschweig experiments in the following section.

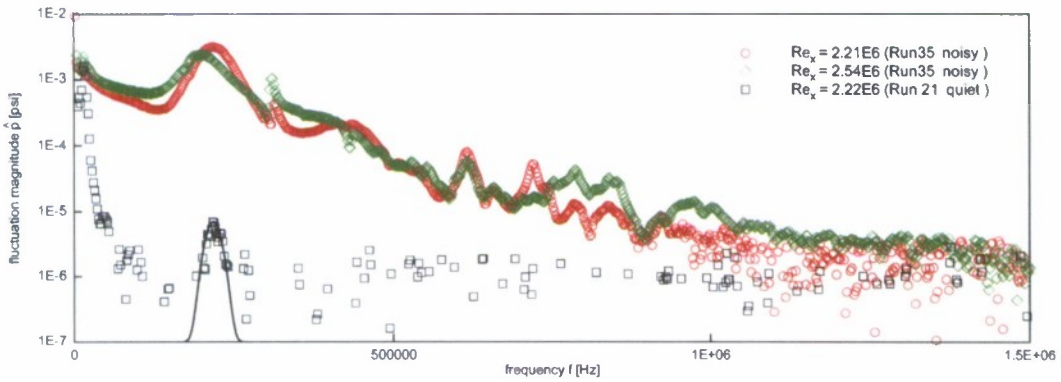

Figure 25: Spectra of pressure fluctuations measured in noisy and quiet flow at same Reynolds numbers

Figure 25 plots the data of Figs. 23a and 24a together using a logarithmic scale. The logarithmic plot shows that in the transitional boundary layer both the lower and higher frequency portions of the spectrum are starting to fill in. However, it is not yet possible to determine how much of the difference in spectra is due to nonlinear amplification and breakdown of the waves, and how much is due to the difference in the spectrum of the free-stream noise.

Since under quiet flow at this pressure the second mode is just becoming detectable, the measurement technique does not permit comparing linear amplification rates at the same Reynolds number in quiet and noisy hypersonic flow. It will be necessary to use controlled perturbations in the quiet-flow boundary layer to make such a comparison.

Figure 26 shows normalized pressure spectra measured at the cone surface at two different Reynolds numbers compared to a measured Pitot pressure spectrum. The surface pressure spectrum at the higher Reynolds number is the one from Figure 24b at $x = 340$ mm which is just before stagnation of the second-mode growth. Note that the Pitot spectrum was measured with an absolute pressure sensor providing the actual mean pressure for normalization. On the other hand, the surface pressure spectra were normalized with the edge pressure calculated from inviscid conical flow solution at M = 5.8 for the measured

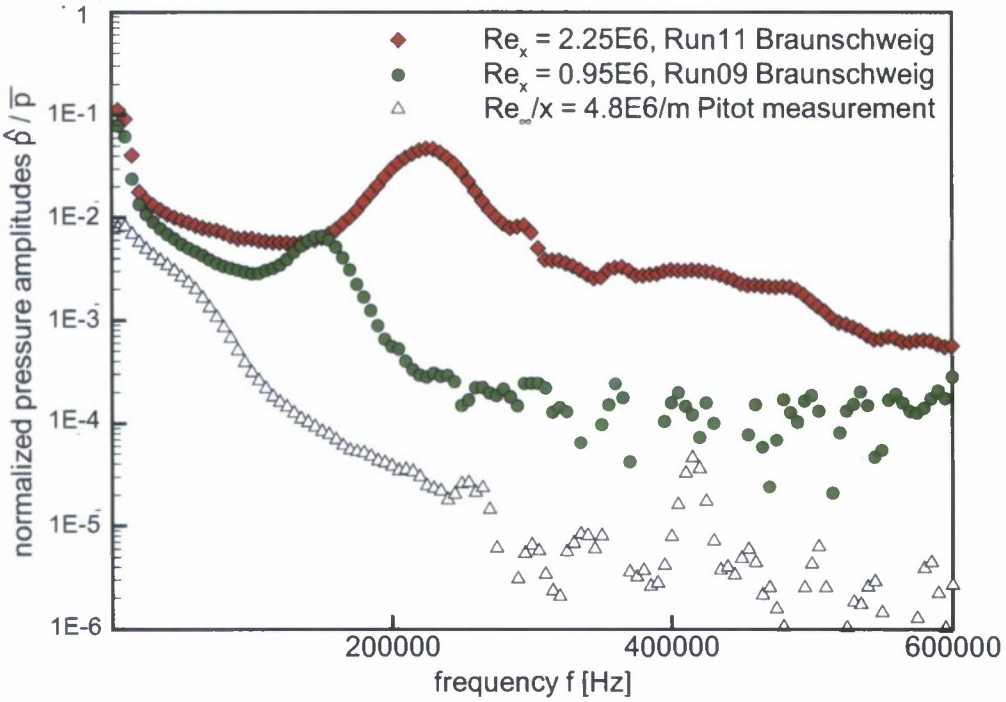

Figure 26: Surface pressure fluctuations normalized by calculated edge pressures at two different Reynolds numbers compared to normalized Pitot pressure fluctuations measured in the Braunschweig tunnel

stagnation pressure. Therefore the normalization of the surface pressure spectra is somewhat uncertain. However, the normalized surface pressure fluctuations are higher than the Pitot fluctuations by almost a factor 2, even at low frequencies. The reason for that difference is not clear. An effect of receptivity or an early amplification of disturbances within the cone boundary-layer can be suspected (see also Ref. [45]).

Often rms values of pressure measurements are used to compare noise levels, although this quantity does not give any information on the spectral distribution of the fluctuations. However, in order to give some idea of how much the rms of the fluctuations rises before transition occurs it may be of interest to provide the rms values for the three measurements shown in Figure 26: rms($\triangle$) = 1.4%; rms($\bigcirc$) = 6.7%; rms($\diamond$) = 13%.

8.2 Measurements of Second-Mode Instabilities Using ALTP Gauges

A group led by Stuttgart University in Germany has led the development of fast-response high-sensitivity heat-flux gauges [26, 46]. The Atomic Layer Thermopile (ALTP) gauge uses the transverse Seeback effect in a crystal of yttrium-barium-copper oxide, as described in detail in Refs. [47] and [48]. The gauge is manufactured in small quantities as an optical detector. Ref. [47] states that the sensors are linear over more than 11 orders of magnitude, and that heat flux was detected at rates varying from a few mW/cm^2 up to 20 kW/cm^2. The maximum frequency response varies from about 250 kHz to about 1 MHz, depending

on how the sensors are manufactured.

The ALTP gauges have successfully been used to measure second-mode waves in the tunnels at Purdue (both quiet and noisy), at Braunschweig, and in Russia. Since the heat-transfer rates in the Purdue tunnel are low, due to the relatively low stagnation temperature of about 430K, the sensitivity is limited. The ALTP gauges show particular promise for high-enthalpy facilities with higher heat-transfer rates, and perhaps for flight experiments. However, they are not yet available commercially, so currently available information is limited to the work of the Stuttgart-led group.

9 Summary

The Mach-6 Ludwieg tube at Purdue is now running quiet with good reliability, to unit Reynolds numbers of about 3.5×10^6/ft. Quiet flow provides low noise levels comparable to flight, and 1-2 orders of magnitude smaller than those in conventional tunnels. This long-sought capability offers a method of studying many critical phenomena which will take many years to investigate.

Measurements on sharp cones and the X-51A show that smooth-wall transition is affected by tunnel noise, as has been long known. For transition induced by isolated roughness, it was long thought that tunnel noise would have an effect only for roughnesses that were less than 'effective'. However, measurements on the 7-deg. cone show that transition is a factor of two farther downstream under quiet flow, even for 'effective' roughness.

No single ground facility can simulate all aspects of hypervelocity flight. Reliable prediction methods for transition in flight will have to be based on approximate simulations of the transition mechanisms. These simulations must be developed and validated using experiments in various wind tunnels. Two robust flush-surface sensors have successfully detected second-mode instability waves in the Mach-6 quiet tunnel, opening a path for more such measurements in other facilities. Under quiet flow, the amplitude of second-mode waves on a 7-deg. sharp cone was about 450 times smaller than under noisy flow, even though the broadband pitot noise was only about 50-100 times smaller. In addition, transition induced by second-mode waves under noisy flow occurred at about the same Reynolds number and wave amplitude in the Ludwieg tubes at Purdue and Braunschweig, despite their differing noise characteristics. This suggests that nonlinear breakdown may not be too sensitive to the details of the background noise field.

For three-dimensional flowfields, the crossflow instability may often dominate. With moderate surface roughness and low freestream noise, stationary waves may dominate traveling waves, as at low speed on swept wings. However, measurements on a cone at angle of attack under quiet flow show a clear effect of tunnel noise on transition that is apparently induced by the stationary crossflow waves; perhaps this is due to the effect of the tunnel noise on the secondary instability. It has been difficult to determine the characteristics of the surface roughness pattern that affect stationary crossflow waves on a cone at angle of attack. However, recent measurements on the HIFiRE-5 elliptic cone show a clear effect of surface roughness on crossflow-induced transition. Continuing research should therefore be able to determine which aspects of the roughness affect transition, opening up the way to controlled studies of crossflow-induced transition at high speeds.

10 Acknowledgements

Most of the present report is edited from the cited papers, each of which has multiple authors. Portions of the work were also supported by Sandia National Laboratories under contract 858548 and by various NASA grants. Since all these grants support related work in the Mach-6 quiet tunnel, they are synergistic in many ways, but an attempt has been made to isolated the AFOSR-supported work in the present report. These complex quiet-tunnel experiments would not have been possible without the support of many organizations and individuals. The measurements reported here were carried out by the following graduate students doing thesis work in the Mach-6 tunnel: Shann Rufer, Erick Swanson, Matt Borg, Tom Juliano, and Katya Casper. Malte Estorf made very useful measurements with the PCB sensors while visiting from T.U. Braunschweig using German government support. The work of H. Knauss and T. Roediger was also supported by the German government.

11 References

[1] Guy Norris. Falcon Force. *Aviation Week and Space Technology*, 2008. 19 May issue, p. 70.

[2] Matthew P. Borg and Steven P. Schneider. Effect of freestream noise on instability and transition for the X-51A lee side. Paper 2009-0396, AIAA, January 2009.

[3] Steven P. Schneider, Thomas J. Juliano, and Matthew P. Borg. High-Reynolds-number laminar flow in the Mach-6 quiet-flow Ludwieg tube. Paper 2006-3056, AIAA, June 2006.

[4] Shann J. Rufer and Steven P. Schneider. Hot-wire measurements of instability waves on cones at Mach 6. Paper 2006-3054, AIAA, June 2006.

[5] Thomas J. Juliano, Erick O. Swanson, and Steven P. Schneider. Transition research and improved performance in the Boeing/AFOSR Mach-6 quiet tunnel. Paper 2007-0535, AIAA, January 2007.

[6] Steven P. Schneider and Thomas J. Juliano. Laminar-turbulent transition measurements in the Boeing/AFOSR Mach-6 quiet tunnel. Paper 2007-4489, AIAA, June 2007.

[7] Matthew P. Borg, Steven P. Schneider, and Thomas J. Juliano. Effect of freestream noise on roughness-induced transition for the X-51A forebody. Paper 2008-0592, AIAA, January 2008.

[8] Malte Estorf, Rolf Radespiel, Steven P. Schneider, Heath B. Johnson, and Stefan Hein. Surface-pressure measurements of second-mode instability in quiet hypersonic flow. Paper 2008-1153, AIAA, January 2008.

[9] Timothy Roediger, Helmut Knauss, Ewald Kramer, Malte Estorf, and Steven P. Schneider. Hypersonic instability waves measured using fast-response heat-flux gauges. Paper 2008-0638, AIAA, January 2008.

[10] Thomas J. Juliano, Rodrigo Segura, Matthew P. Borg, Katya Casper, Michael J. Hannon, Jr, Brad M. Wheaton, and Steven P. Schneider. Starting issues and forward-facing cavity resonance in a hypersonic quiet tunnel. Paper 2008-3735, AIAA, June 2008.

[11] Katya M. Casper, Brad M. Wheaton, Heath B. Johnson, and Steven P. Schneider. Effect of freestream noise on roughness-induced transition at Mach 6. Paper 2008-4291, AIAA, June 2008.

[12] Hadassah Naiman, Doyle D. Knight, Selin Aradag, Thomas J. Juliano, and Steven P. Schneider. Performance improvements in the Boeing/AFOSR Mach-6 quiet wind tunnel based on CFD predictions. In *Third International Symposium on Integrating CFD and Experiments in Aerodynamics*, U.S. Air Force Academy, Colorado, June 2007.

[13] Thomas J. Juliano and Steven P. Schneider. Laminar-turbulent transition on the HTV-2 in a Mach-6 quiet tunnel. Paper 8-2, AIAA, November 2008. Presented at the AIAA Missile Sciences Conference in Monterey. The distribution of the paper is limited, but the title appeared in the public-release agenda.

[14] Steven P. Schneider. Effects of roughness on hypersonic boundary-layer transition. Paper 2007-0305, AIAA, January 2007.

[15] Steven P. Schneider. The development of hypersonic quiet tunnels. Paper 2007-4486, AIAA, June 2007.

[16] Steven P. Schneider. Hypersonic boundary-layer transition on blunt bodies with roughness. Paper 2008-0501, AIAA, January 2008.

[17] Steven P. Schneider. Hypersonic boundary-layer transition with ablation and blowing. Paper 2008-3730, AIAA, June 2008.

[18] Selin Aradag, Doyle D. Knight, and Steven P. Schneider. Bleed lip geometry effects on the flow in a hypersonic wind tunnel. *AIAA Journal*, 44(9):2133–2136, Sept. 2006.

[19] Ezgi S. Taskinoglu, Doyle D. Knight, and Steven P. Schneider. Computational fluid dynamics evaluation of bleed slot of the Purdue Mach 6 quiet tunnel. *AIAA Journal*, 44(6):1360–1362, June 2006.

[20] Terry R. Salyer, Steven H. Collicott, and Steven P. Schneider. Characterizing laser-generated hot spots for receptivity studies. *AIAA Journal*, 44(12):2871–2878, December 2006.

[21] Thomas J. Juliano, Steven P. Schneider, Selin Aradag, and Doyle Knight. Quiet-flow Ludwieg tube for hypersonic transition research. *AIAA Journal*, 46(7):1757–1763, July 2008.

[22] Steven P. Schneider. Effects of roughness on hypersonic boundary-layer transition. *Journal of Spacecraft and Rockets*, 45(2):193–209, Mar.-Apr. 2008.

[23] Steven P. Schneider. Development of hypersonic quiet tunnels. *Journal of Spacccraft and Rockets*, 45(4):641–664, Jul.-Aug. 2008.

[24] Steven P. Schneider. Hypersonic boundary-layer transition on blunt bodies with roughness. *Journal of Spacecraft and Rockets*, 45(6):1090–1105, Nov.-Dec. 2008.

[25] Matthew P. Borg and Steven P. Schneider. Effect of freestream noise on roughness-induced transition for the X-51A forebody. *J. Spacecraft and Rockets*, 45(6):1106–1116, Nov.-Dec. 2008.

[26] Timothy Roediger, Helmut Knauss, Malte Estorf, Steven P. Schneider, and M.V. Smorodsky. Hypersonic instability waves measured using fast-response heat-flux gauges. *J. of Spacecraft and Rockets*, 46(2):266–273, March-April 2009.

[27] Erick O. Swanson. *Boundary-Layer Transition on Cones at Angle of Attack in a Mach-6 Quiet Tunnel.* PhD thesis, School of Aeronautics and Astronautics, Purdue University, May 2008.

[28] Thomas J. Juliano. Nozzle modifications for high-Reynolds-number quiet flow in the Boeing/AFOSR Mach-6 quiet tunnel. Master's thesis, School of Aeronautics and Astronautics, Purdue University, December 2006. Completed in October with contents current through August 2006. DTIC citation AD-A456772.

[29] Rodrigo Segura. Oscillations in a forward-facing cavity measured using laser-differential interferometry in a hypersonic quiet tunnel. Master's thesis, School of Aeronautics and Astronautics, Purdue University, December 2007. DTIC citation AD-A474770.

[30] I.E. Beckwith and C.G. Miller III. Aerothermodynamics and transition in high-speed wind tunnels at NASA Langley. *Annual Review of Fluid Mechanics*, 22:419–439, 1990.

[31] S. P. Schneider and C. E. Haven. Quiet-flow Ludwieg tube for high-speed transition research. *AIAA Journal*, 33(4):688–693, April 1995.

[32] Steven P. Schneider, Craig Skoch, Shann Rufer, Shin Matsumura, and Erick Swanson. Transition research in the Boeing/AFOSR Mach-6 quiet tunnel. Paper 2002-0302, AIAA, January 2002.

[33] Steven P. Schneider, Craig Skoch, Shann Rufer, Erick Swanson, and Matt Borg. Bypass transition on the nozzle wall of the Boeing/AFOSR Mach-6 quiet tunnel. Paper 2004-0250, AIAA, January 2004.

[34] Steven P. Schneider. Hypersonic laminar-turbulent transition on circular cones and scramjet forebodies. *Progress in Aerospace Sciences*, 40(1-2):1–50, 2004.

[35] S. P. Wilkinson, S. G. Anders, and F.-J. Chen. Status of Langley quiet flow facility developments. Paper 94-2498, AIAA, June 1994.

[36] Scott Berry, Aaron Auslender, Arthur D. Dilley, and John Calleja. Hypersonic boundary-layer trip development for Hyper-X. *Journal of Spacecraft and Rockets*, 38(6):853–864, Nov.-Dec. 2001.

[37] Steven P. Schneider, Steven H. Collicott, J.D. Schmisseur, Dale Ladoon, Laura A. Randall, Scott E. Munro, and T.R. Salyer. Laminar-turbulent transition research in the Purdue Mach-4 quiet-flow Ludwieg tube. Paper 96-2191, AIAA, June 1996.

[38] Scott Berry and Thomas Horvath. Discrete roughness transition for hypersonic flight vehicles. *J. of Spacecraft and Rockets*, 45(2):216–227, March-April 2008.

[39] Steven P. Schneider, Craig Skoch, Shann Rufer, Erick Swanson, and Matthew P. Borg. Laminar-turbulent transition research in the Boeing/AFOSR Mach-6 quiet tunnel. Paper 2005-0888, AIAA, January 2005.

[40] Steven P. Schneider, Craig Skoch, Shann Rufer, and Erick Swanson. Hypersonic transition research in the Boeing/AFOSR Mach-6 quiet tunnel. Paper 2003-3450, AIAA, June 2003.

[41] Mujeeb R. Malik, Fei Li, Meelan M. Choudhari, and Chau lyan Chang. Secondary instability of crossflow vortices and swept-wing boundary-layer transition. *Journal of Fluid Mechanics*, 399:85–115, 1999.

[42] R.H. Radeztsky, M.S. Reibert, and W.S. Saric. Effect of isolated micron-sized roughness on transition in swept-wing flows. *AIAA J.*, 37(11):1370–1377, November 1999.

[43] Karen T. Berger, Shann J. Rufer, Roger Kimmel, and David Adamczak. Aerothermodynamic characteristics of boundary layer transition and trip effectiveness on the HIFiRE flight 5 vehicle. Paper 2009-XXXX, AIAA, June 2009. Submitted to the AIAA conference.

[44] Keisuke Fujii. Experiment of two dimensional roughness effect on hypersonic boundary layer transition. *Journal of Spacecraft and Rockets*, 43(4):731–738, July-August 2006.

[45] M.R. Schopper. Interaction of aerodynamic noise with laminar boundary layers in supersonic wind tunnels. Technical Report CR-3621, NASA, April 1984.

[46] D. Heitmann, C.J. Kaehler, R. Radespiel, T. Roediger, H. Knauss, and E. Kraemer. Disturbance-level and roughness-induced transition measurements in a conical boundary layer at Mach 6. Paper 2008-3951, AIAA, June 2008.

[47] Tim Roediger, Helmut Knauss, Uwe Gaisbauer, Ewald Kraemer, Sean Jenkins, and Jens von Wolfersdorf. Time-resolved heat transfer measurements on the tip wall of a ribbed channel using a novel heat flux sensor – Part I: Sensor and benchmarks. *ASME Journal of Turbomachinery*, 130:011018–1 to 011018–8, January 2008.

[48] Helmut Knauss, Timothy Roediger, Dimitry A. Bountin, Boris V. Smorodsky, Anatoly A. Maslov, and Julio Srulijes. A novel sensor for fast heat-flux measurements. *J. of Spacecraft and Rockets*, 46(2):255–265, March-April 2009.